Kybernetika

Cong Thang Pham; Thi Thu Thao Tran

An algorithm for hybrid regularizers based image restoration with Poisson noise

Kybernetika, Vol. 57 (2021), No. 3, 446–473

Persistent URL: http://dml.cz/dmlcz/149201

KYBERNETIKA — VOLUME 57 (2021), NUMBER 3, PAGES 446–473

AN ALGORITHM FOR HYBRID REGULARIZERS BASED IMAGE RESTORATION WITH POISSON NOISE

Cong Thang Pham and Thi Thu Thao Tran

In this paper, a hybrid regularizers model for Poissonian image restoration is introduced. We study existence and uniqueness of minimizer for this model. To solve the resulting minimization problem, we employ the alternating minimization method with rigorous convergence guarantee. Numerical results demonstrate the efficiency and stability of the proposed method for suppressing Poisson noise.

Keywords: total variation, image denoising, image deblurring, alternating minimization method

Classification: 35A15, 94A08

1. INTRODUCTION

The restoration of clean images from observations is a fundamental task in the image processing and computer vision. The challenging task for image denoising is to remove noise and to preserve fine details [26]. Image restoration is often formulated as the problem of reconstructing the clean image z with the size of $M \times N$ damaged by some noise η, from the observed image $f = f(x)$ with $x = (x_1; x_2) \in \Omega, \Omega \subseteq \mathbb{R}^2$ being an open bounded domain. In recent years, many methods image denoising have been proposed for Gaussian white noise. However, in photon-counting devices, such as radiography, astronomical imaging, electronic microscopy [2, 8, 11, 31], images may be corrupted by Poisson noise. Poisson noise is not additive, and it is image pixel-intensity dependent, i. e. bright pixels are statistically more corrupted than dark pixels [5]. The restoration models and methods proposed for Gaussian white noise are not effective in removing Poisson noise [27].

For many years, many variational methods have been proposed to handle the restoration problem with Poisson noise. One of variational models for Poissonian image reconstruction is the one based on the Total Variation (TV) norm as regularization term [15]:

$$z^* = \underset{z \in BV(\Omega)}{\arg\min} \int_\Omega |\nabla z| \, \mathrm{d}x + \beta \int_\Omega (z - f \log z) \, \mathrm{d}x, \tag{1}$$

DOI: 10.14736/kyb-2021-3-0446

where $\beta > 0$ is a regularization parameter, z must be positive in Ω, $\int_\Omega |\nabla z| \, \mathrm{d}x$ stands for the total variation of z, the operator $|\nabla z|$ is defined later (cf. eq. 8), and BV is the space of functions with bounded variation.

In case of the blur effect, authors in [20, 33] studied a penalized likelihood approach with TV penalty for Poissonian image denoising and deblurring as follows:

$$z^* = \underset{z \in BV(\Omega), \log Kz \in L^1(\Omega)}{\arg\min} \int_\Omega |\nabla z| \, \mathrm{d}x + \beta \int_\Omega (Kz - f \log Kz) \, \mathrm{d}x, \tag{2}$$

where K being a nonnegative linear compact operator; $\beta > 0$ is a regularization parameter, z must be positive in Ω.

In recent years, many effective numerical algorithms have proposed for solving problem 2, for instance, EM–TV algorithm [32, 34], split Bregman iteration [6, 33], alternating minimization method [18, 20, 21, 36, 37], Liu and Huang in [19] proposed another new total bounded variation-based Poissonian images restoration model as follows:

$$z^* = \underset{z \in BV(\Omega)}{\arg\min} \int_\Omega |\nabla z| \, \mathrm{d}x + \frac{\lambda}{2} \|z\|_2^2 + \beta \int_\Omega (Kz - f \log Kz) \, \mathrm{d}x, \tag{3}$$

where $\beta > 0$ is a regularization parameter, z must be positive in Ω. The authors extended split Bregman iteration to obtain the optimal solution recursively.

The model 3 performs very well for preserving edges while removing noise. However, it often causes undesired staircase effects in smooth regions. To overcome the staircase effects, some high-order models have been introduced for restoring blurred images corrupted by Poisson noise. The authors in [35] replaced the TV term in 3 with second-order TV as $\nabla^2 z$ (cf. Eq. 9) and employed a split Bregman algorithm to solve their model. Authors in [13] proposed the hybrid higher-order TV model to restore images corrupted by blur and Poisson noise as follows:

$$z^* = \underset{z \in S(\Omega)}{\arg\min} \left(\int_\Omega \gamma \, |\nabla z| \, \mathrm{d}x + \int_\Omega (1 - \gamma) \, |\nabla^2 z| \, \mathrm{d}x + \beta \int_\Omega (Kz - f \log Kz) \, \mathrm{d}x \right). \tag{4}$$

The authors employed a gradient descent method for computing the minimizer of the model 4. To speed the computation, the same authors converted this optimization model 4 to a constrained problem by variable splitting and addressed it with the alternating direction method in [14].

Inspired by models 3, and 4, we introduce an adaptive TV based optimization problem as follows:

$$z^* = \underset{z \in S(\Omega)}{\arg\min} \left(\int_\Omega \gamma \, |\nabla z| \, \mathrm{d}x + \int_\Omega \alpha \, |\nabla^2 z| \, \mathrm{d}x + \frac{\lambda}{2} \|z\|_2^2 + \beta \int_\Omega (Kz - f \log Kz) \, \mathrm{d}x \right), \tag{5}$$

where λ, β - positive regularization parameters, $S(\Omega) = \{z \in BV(\Omega) \cap BV^2(\Omega), z > 0\}$, $\alpha = 1 - \gamma$ and $\gamma \in (0, 1]$ are the weighted parameter.

In this paper, we study an effective method for image restoration corrupted by Poisson noise. We can emphasize that the proposed model is general case of the above mentioned models in [19, 13, 14]. We can emphasize that the proposed model 5 is general case of the models mentioned above. Like model 3, the proposed model 5 contains the quadratic

regularization term $\frac{\lambda}{2}\|z\|_2^2$ which can be guarantee uniqueness of the solution and the convergence of the proposed algorithm. Like model 4, the proposed model 5 contains a combination of TV and higher order TV as regularization terms. It allows to remove the noise efficiently and preserve the image details, and avoid staircasing artifacts in the restored images.

For our model, we study existence and uniqueness of its solution. We employ the alternating minimization method to compute the resulting minimization problem by introducing new auxiliary variables. The majorization-minimization method is used for solving the subproblems. We also study the convergence of our proposed algorithm. The experimental results show that our algorithm obtains the high efficiency for Poisson noise removal when compared with the well-known methods.

Our paper is organized as follows. In section 2, the proposed method is presented. In section 3, we perform experiments to show the efficiency of our proposed algorithm. Finally, the conclusions are given in section 4.

2. THE PROPOSED METHOD

Definitions and notations of the spaces BV and BV^2 space can be found in [1, 7, 9, 16, 17, 24]. The existence and uniqueness of the minimizer for the proposed model 5 are established by Theorem 1.

Theorem 1. Assume that f is a positive bounded function and K is injective, then the problem 5 is strictly convex and the problem 5 for $z \in BV(\Omega) \cap BV^2(\Omega)$ such that $\log z \in L^1(\Omega)$ has a unique minimizer.

The proof follows reasoning similar to the proof of [13, 19, 35], thus omitted.

In this section, we derive the numerical method for problem 5 in detail. We introduce three new variables (d, g, q) and rewrite 5 in the constrained optimization problem as follows:

$$\min_{z,d,g,q} \Big(\gamma\|d\|_1 + \alpha\|g\|_1 + \frac{\lambda}{2}\|z\|_2^2 + \beta\langle 1, q - f\log q\rangle\Big) \quad \text{s.t. } d = \nabla z, g = \nabla^2 z, q = Kz. \tag{6}$$

The augmented Lagrangian functional for the constrained optimization problem 6 is defined as:

$$\begin{aligned}\mathcal{L}(z,d,g,q,\rho_1,\rho_2,\rho_3) = \Big(&\gamma\|d\|_1 + \alpha\|g\|_1 + \frac{\lambda}{2}\|z\|_2^2 + \beta\langle 1, q - f\log q\rangle \\ &- \langle\rho_1, d - \nabla z\rangle + \frac{\eta_1}{2}\|d - \nabla z\|_2^2 - \langle\rho_2, g - \nabla^2 z\rangle + \frac{\eta_2}{2}\|g - \nabla^2 z\|_2^2 \\ &- \langle\rho_3, q - Kz\rangle + \frac{\eta_3}{2}\|q - Kz\|_2^2\Big),\end{aligned} \tag{7}$$

where η_1, η_2, η_3 - positive parameters; ρ_1, ρ_2, ρ_3 - with Lagrangian multipliers.

The discrete gradient ∇z and the second-order derivatives $\nabla^2 z$ of an image z for the pixel location (i, j) in z $(i = 1..M; j = 1..N)$ are defined like [28, 29, 30]:

$$\nabla_x z_{i,j} = z_{i+1,j} - z_{i,j}\ , \quad \nabla_y z_{i,j} = z_{i,j+1} - z_{i,j},$$

$$\nabla z_{i,j} = (\nabla_x z_{i,j}, \nabla_y z_{i,j}), \quad |\nabla z_{i,j}| = \sqrt{(\nabla_x z_{i,j})^2 + (\nabla_y z_{i,j})^2}, \tag{8}$$

$$\nabla_{xx} z_{i,j} = z_{i+1,j} - 2z_{i,j} + z_{i-1,j}, \quad \nabla_{yy} z_{i,j} = z_{i,j+1} - 2z_{i,j} + z_{i,j-1},$$

$$\nabla_{xy} z_{i,j} = \nabla_{yx} z_{i,j} = z_{i,j} - z_{i,j-1} - z_{i-1,j} + z_{i-1,j-1},$$

$$\left|\nabla^2 z\right| = \sqrt{(\nabla_{xx} z_{i,j})^2 + (\nabla_{xy} z_{i,j})^2 + (\nabla_{yx} z_{i,j})^2 + (\nabla_{yy} z_{i,j})^2}. \tag{9}$$

Then, using the alternating minimization method to solve the problem 7 can be expressed as follows:

$$\begin{cases} z^{(k+1)} = \arg\min_z \Big(\frac{\lambda}{2}\|z\|_2^2 - \langle \rho_1^{(k)}, d^{(k)} - \nabla z\rangle + \frac{\eta_1}{2}\|d^{(k)} - \nabla z\|_2^2 - \\ \langle \rho_2^{(k)}, g^{(k)} - \nabla^2 z\rangle + \frac{\eta_2}{2}\|g^{(k)} - \nabla^2 z\|_2^2 - \langle \rho_3^{(k)}, q^{(k)} - Kz\rangle + \frac{\eta_3}{2}\|q^{(k)} - Kz\|_2^2 \Big), \\ d^{(k+1)} = \arg\min_d \Big(\gamma\|d\|_1 - \langle \rho_1, d - \nabla z^{(k+1)}\rangle + \frac{\eta_1}{2}\|d - \nabla z^{(k+1)}\|_2^2 \Big), \\ g^{(k+1)} = \arg\min_g \Big(\alpha\|g\|_1 - \langle \rho_2^{(k)}, g - \nabla^2 z^{(k+1)}\rangle + \frac{\eta_2}{2}\|g - \nabla^2 z^{(k+1)}\|_2^2 \Big), \\ q^{(k+1)} = \arg\min_q \Big(\beta\langle 1, q - f\log q\rangle - \langle \rho_3^{(k)}, q - Kz^{(k+1)}\rangle + \frac{\eta_3}{2}\|q - Kz^{(k+1)}\|_2^2 \Big), \end{cases} \tag{10}$$

with update for $\rho_1^{(k+1)}, \rho_2^{(k+1)}, \rho_3^{(k+1)}$:

$$\begin{cases} \rho_1^{(k+1)} = \rho_1^{(k)} + \eta_1(\nabla z^{(k+1)} - d^{(k+1)}), \\ \rho_2^{(k+1)} = \rho_2^{(k)} + \eta_2(\nabla^2 z^{(k+1)} - g^{(k+1)}), \\ \rho_3^{(k+1)} = \rho_3^{(k)} + \eta_3(Kz^{(k+1)} - q^{(k+1)}). \end{cases} \tag{11}$$

— The z subproblem in 10 is given by:

$$\begin{aligned} z^{(k+1)} &= \arg\min_z \Big(\frac{\lambda}{2}\|z\|_2^2 - \langle \rho_1^{(k)}, d^{(k)} - \nabla z\rangle + \frac{\eta_1}{2}\|d^{(k)} - \nabla z\|_2^2 \\ &- \langle \rho_2^{(k)}, g^{(k)} - \nabla^2 z\rangle + \frac{\eta_2}{2}\|g^{(k)} - \nabla^2 z\|_2^2 - \langle \rho_3^{(k)}, q^{(k)} - Kz\rangle + \frac{\eta_3}{2}\|q^{(k)} - Kz\|_2^2 \Big) \\ &= \arg\min_z \Big(\frac{\lambda}{2}\|z\|_2^2 + \frac{\eta_1}{2}\|d^{(k)} - \nabla z - \frac{\rho_1^{(k)}}{\eta_1}\|_2^2 + \frac{\eta_2}{2}\|g^{(k)} - \nabla^2 z - \frac{\rho_2^{(k)}}{\eta_2}\|_2^2 \\ &+ \frac{\eta_3}{2}\|q^{(k)} - Kz - \frac{\rho_3^{(k)}}{\eta_3}\|_2^2 \Big). \end{aligned}$$

Thus, we get:

$$\begin{aligned} &\lambda z + \eta_1 \nabla^T \Big(\nabla z + \frac{\rho_1^{(k)}}{\eta_1} - d^{(k)}) + \eta_2 \nabla^{2^T} (\nabla^2 z + \frac{\rho_2^{(k)}}{\eta_2} - g^{(k)} \Big) \\ &+ \eta_3 K^T \Big(Kz + \frac{\rho_3^{(k)}}{\eta_3} - q^{(k)} \Big) = 0. \end{aligned} \tag{12}$$

We can rewrite the equation 12 as:

$$\begin{aligned}&\left(\lambda+\eta_1\nabla^T\nabla+\eta_2{\nabla^2}^T\nabla^2+\eta_3K^TK\right)z^{(k+1)}\\&=\eta_1\nabla^T\left(d^{(k)}-\frac{\rho_1^{(k)}}{\eta_1}\right)+\eta_2{\nabla^2}^T\left(g^{(k)}-\frac{\rho_2^{(k)}}{\eta_2}\right)+\eta_3K^T\left(q^{(k)}-\frac{\rho_3^{(k)}}{\eta_3}\right).\end{aligned}\tag{13}$$

In system 13, we can note that $KK^T, \nabla\nabla^T, \nabla^2{\nabla^2}^T$ are all block circulant under the periodic boundary condition, so that they can be diagonalized by by fast Fourier transform (FFT). Hence, $z^{(k+1)}$ can be calculated by FFT and inverse FFT efficiently:

$$z^{(k+1)}=\mathcal{F}^{-1}\Big(\frac{\mathcal{F}\Big(\eta_1\nabla^T(d^{(k)}-\frac{\rho_1^{(k)}}{\eta_1})+\eta_2{\nabla^2}^T(g^{(k)}-\frac{\rho_2^{(k)}}{\eta_2})+\eta_3K^T(q^{(k)}-\frac{\rho_3^{(k)}}{\eta_3})\Big)}{\lambda+\eta_1\mathcal{F}\big(\nabla^T\nabla\big)+\eta_2\mathcal{F}\big({\nabla^2}^T\nabla^2\big)+\eta_3\mathcal{F}\big(K^TK\big)}\Big),\tag{14}$$

where $\mathcal{F}$ and $\mathcal{F}^{-1}$ are the forward and inverse Fourier transform operators.

— The d subproblem is given by:

$$\begin{aligned}d^{(k+1)}&=\arg\min_d\Big(\gamma\|d\|_1-\langle\rho_1,d-\nabla z^{(k+1)}\rangle+\frac{\eta_1}{2}\|d-\nabla z^{(k+1)}\|_2^2\Big)\\&=\arg\min_d\Big(\gamma\|d\|_1+\frac{\eta_1}{2}\|d-\nabla z^{(k+1)}-\frac{\rho_1^{(k)}}{\eta_1}\|_2^2\Big).\end{aligned}$$

The solution of the d subproblem can readily be obtained by applying the soft thresholding operator [23]:

$$d^{(k+1)}=\frac{\nabla z^{(k+1)}+\frac{\rho_1^{(k)}}{\eta_1}}{\left|\nabla z^{(k+1)}+\frac{\rho_1^{(k)}}{\eta_1}\right|}\cdot\max\left(\left|\nabla z^{(k+1)}+\frac{\rho_1^{(k)}}{\eta_1}\right|-\frac{\gamma}{\eta_1},0\right).\tag{15}$$

— The g subproblem is given by:

$$\begin{aligned}g^{(k+1)}&=\arg\min_g\Big(\alpha\|g\|_1-\langle\rho_2^{(k)},g-\nabla^2z^{(k+1)}\rangle+\frac{\eta_2}{2}\|g-\nabla^2z^{(k+1)}\|_2^2\Big)\\&=\arg\min_g\left(\alpha\|g\|_1+\frac{\eta_2}{2}\|g-\nabla^2z^{(k+1)}-\frac{\rho_2^{(k)}}{\eta_2}\|_2^2\right).\end{aligned}$$

The solution of the g subproblem can be obtained by applying the soft thresholding operator too:

$$g^{(k+1)}=\frac{\nabla^2z^{(k+1)}+\frac{\rho_2^{(k)}}{\eta_2}}{\left|\nabla^2z^{(k+1)}+\frac{\rho_2^{(k)}}{\eta_2}\right|}\cdot\max\left(\left|\nabla^2z^{(k+1)}+\frac{\rho_2^{(k)}}{\eta_2}\right|-\frac{\alpha}{\eta_2},0\right).\tag{16}$$

— The q subproblem is given by:

$$q^{(k+1)} = \arg\min_q \left(\beta\langle 1, q - f\log q\rangle - \langle \rho_3^{(k)}, q - Kz^{(k+1)}\rangle + \frac{\eta_3}{2}\|q - Kz^{(k+1)}\|_2^2 \right)$$
$$= \arg\min_q \left(\beta\langle 1, q - f\log q\rangle + \frac{\eta_3}{2}\|q - Kz^{(k+1)} - \frac{\rho_3^{(k)}}{\eta_3}\|_2^2 \right).$$

Therefore, we get:

$$\beta(1 - \frac{f}{q}) + \eta_3(q - Kz^{(k+1)}) - \rho_3^{(k)} = 0.$$

This equation can be rewritten as follows:

$$\eta_3 q^2 - q(\eta_3 Kz^{(k+1)} + \rho_3^{(k)} - \beta) - \beta f = 0.$$

The solution of $q^{(k+1)}$ is the positive solution given by:

$$q^{(k+1)} = \frac{(\eta_3 Kz^{(k+1)} + \rho_3^{(k)} - \beta) + \sqrt{(\eta_3 Kz^{(k+1)} + \rho_3^{(k)} - \beta)^2 + 4\eta_3\beta f}}{2\eta_3}. \tag{17}$$

The complete method is summarized in **Algorithm 1**.

Algorithm 1: Alternating minimization method for for solving the model 5

1. Initialize: $z^{(0)} = q^{(0)} = f$; $d^{(0)} = g^{(0)} = 0$; $k = 1$
2. **while** Stopping condition is not satisfied **do**
3. Compute $z^{(k+1)}$ according to 14
4. Compute $d^{(k+1)}$ according to 15
5. Compute $g^{(k+1)}$ according to 16
6. Compute $q^{(k+1)}$ according to 17
7. Update $\rho_1^{(k+1)}$, $\rho_2^{(k+1)}$, $\rho_3^{(k+1)}$ by 11
10. $k = k + 1$
11. **endwhile**
12. **return** z

We need a stopping criterion for the iteration: we end the loop if the maximum number of allowed outer iterations N has been carried out (to guarantee an upper bound on running time) or the following condition is satisfied for some prescribed tolerance ς:

$$ERR = \frac{\|z^{(k)} - z^{(k-1)}\|_2}{\|z^{(k)}\|_2} < \varsigma, \tag{18}$$

where ς is a small positive parameter. For our experiments, we set tolerance in 18 $\varsigma = 0.0001$ and $N = 200$.

Due to the convex property of the proposed model (Theorem 1), the convergence of Algorithm 1 follows from the convergence analysis for the TV-based alternating minimization method [10]. In this paper, we do not repeat the lengthy analysis. However, following the Refs. [12, 19, 25, 35], we have convergence theorem (Theorem 2) for the proposed method.

Theorem 2. Let $\{z^{(k)}, d^{(k)}, g^{(k)}, q^{(k)}, \rho_1^{(k)}, \rho_2^{(k)}, \rho_3^{(k)}\}$ be the sequence generated by the given **Algorithm 1** with any initial guess $\{z^{(0)}, d^{(0)}, g^{(0)}, q^{(0)}, \rho_1^{(0)}, \rho_2^{(0)}, \rho_3^{(0)}\}$ converges to $\{z^*, d^*, g^*, q^*, \rho_1^*, \rho_2^*, \rho_3^*\}$, where z^* is unique minimizer of the problem 5, and this implies $\lim_{k\to\infty} \|z^{(k)}\|_2 = z^*$.

We note that similar convergence theories of the TV-based alternating minimization method can be found in [3, 22, 36, 38].

3. NUMERICAL EXPERIMENTS

In this section, we present some numerical results to illustrate the performance of the proposed model for poisson noise removal. We compare our results with images obtained by other well known approaches, as the total bounded variation regularization model (TBV) [35] and the hybrid higher-order TV model (HOTV)[14]. Additionally, the compared methods are implemented by the state-of-the-art alternating minimization method. The test images are shown in Figure 1.

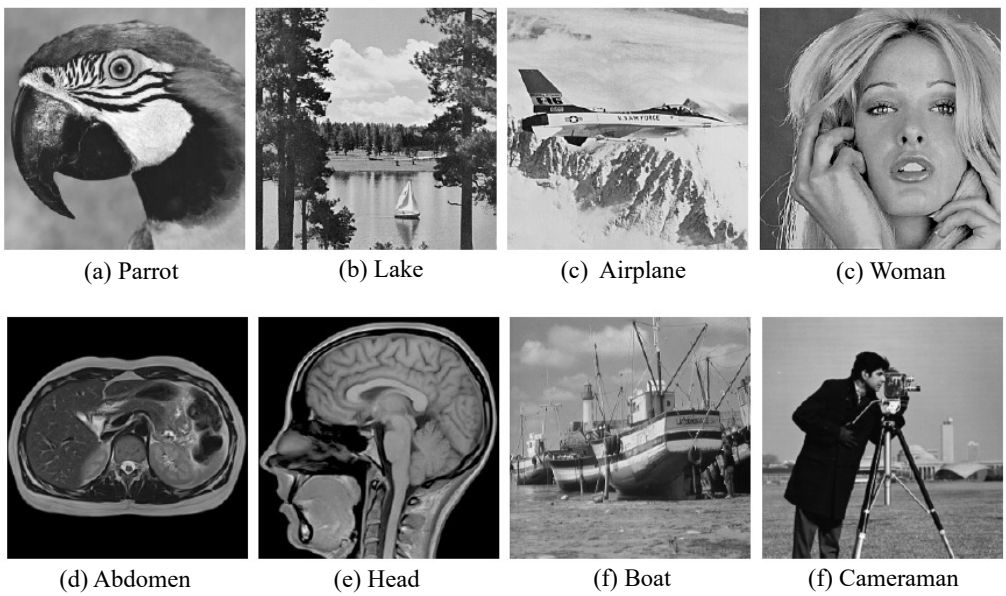

Fig. 1. Test images.

In our numerical implementation, for a fair comparison, all images are processed with the equivalent parameters $\lambda = 0.001$, $\eta_1 = 1.2$, $\eta_2 = 0.1$ and $\eta_3 = 1$. The weighted parameter γ is determined empirically $\gamma = 0.9$ for simplicity and for saving CPU time (see [14] for more details). In each of our experiments, the parameter β is chosen to keep the poise between noise removal and detail preservation capabilities. For a fair comparison, the regularization parameter β depending on concrete experiment is the same value for all compared methods. All experiments were carried out in Windows 10

and Matlab running on a desktop equipped with an Intel Core−i5, 2.4 GHz and 8 GB of RAM.

The quality of the restoration results by the two different methods is compared quantitatively by using the peak signal-to-noise ratio (PSNR):

$$PSNR = 10\log_{10}\left(\frac{255^2 \cdot MN}{\|u^* - u\|_2^2}\right),$$

where u, u^* are the original image, the reconstructed or noisy image accordingly; M and N are the number of image pixels in rows and columns. We also use very popular measure called SSIM. The SSIM measure compares local patterns of pixel intensities normalized for luminance and contrast, and allows us to get more consistent with human visual characteristics [4].

3.1. Image denoising

Our method can perform simultaneously deblurring and denoising, in this section we focus only on the denoising case. Our aim is to recover the original image z with the observed image f. Poisson noise is data-dependent noise, the noise level of observed images depends on the pixel intensity. To generate the noisy images, we first scaled the orginal image u by $u = M \cdot (u/u_{\max})$, where $u_{\max}$ is maximum pixel intensity of image u, M is a specified maximum intensity. Then, we use the Matlab routine $f = poissrnd(u)$.

Optimal selection of the regularization parameter β plays important role in order to achieve an effective restoration results. In order to do this, the regularization parameter β varies from 1 to 50 by steps of 1. We plot the restored PSNR values for compared methods against different values of β. In Figures 2 and 3, we show the PSNR values as a function of regularization parameter β and for the test images. The regularization parameters β for the best for image restoration are summarized in Table 1.

Image	**Parrot**	**Lake**	**Airplane**	**Woman**	**Abdomen**	**Head**	**Boat**	**Cameraman**
Method	$M = 120$							
TBV	10	22	21	19	12	14	19	12
HOTV	12	27	24	21	16	16	21	18
Ours	12	20	17	20	14	15	19	14
-	$M = 60$							
TBV	10	13	12	12	8	9	11	10
HOTV	11	15	11	13	10	11	12	9
Ours	10	12	11	12	7	10	12	10

Tab. 1. The optimal regularization parameter β used for image denoising.

In Figure 4, we present the evolution of ERR (18) as a function of the number of iterations for the compared methods. From this figure, we can see that the error decreases monotonically with iterations. It confirms the convergence behaviour of the compared methods.

We show the denoising results of compared methods in Figures 5, 6 for noise level $M = 120$ and in Figures 7, 8 for noise level $M = 60$, respectively. In these Figures, the

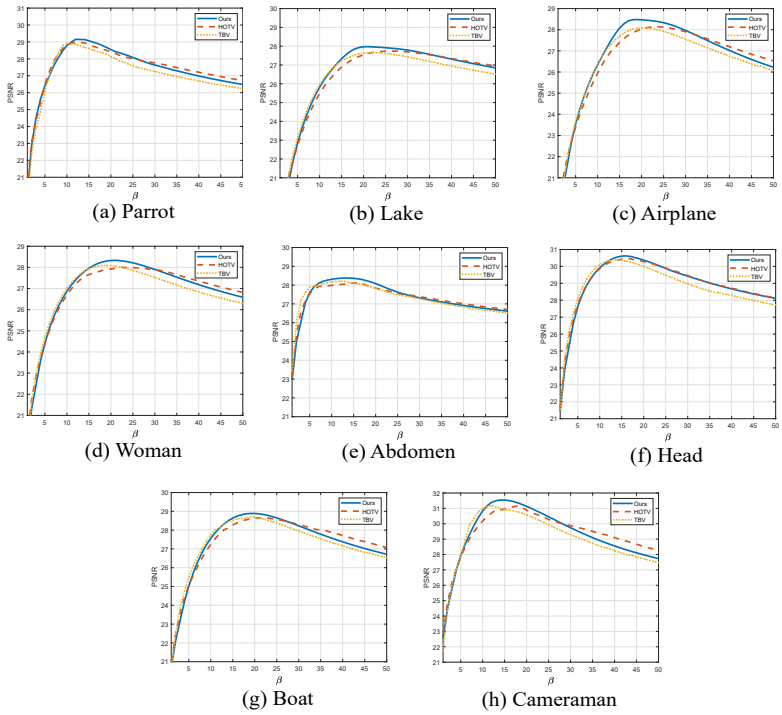

Fig. 2. Plots of the PSNR values versus the values β of the compared methods with noise level $M = 120$.

first columns (a) represent the noisy images, and in the others (b) – (d) separately, we show respectively the reconstructions given by the TBV, the HOTV and our model with their optimal values β from Table 1.

For a better visual comparison, we have enlarged some details of the restored images in Figures 9, 10, 11, and 12 (the first columns include details of the original images). It can be seen that our method gives even better visual quality than other methods.

An important factor to measure the effectiveness of the denoising methods is run time. Table 2 shows the number of iterations and the computational time (in seconds) of the compared methods. We see from the Table 2 that the computation time of the restored images using compared methods is about the same. Furthermore, our proposed method needs less iteration to converge (see Figure 4 for more details).

For the comparison of the performance quantitatively, the measures of PSNR and SSIM values are presented in Table 3 and Table 4. The better restored results are shown in bold. Visually, it can be seen that the reconstruction results of the HOTV model and the TBV model are about the same, and that our model reaches better visual quality and higher PSNR and SSIM values. From figures and tables, we observe that the proposed method is convergent and gets better results than the other methods.

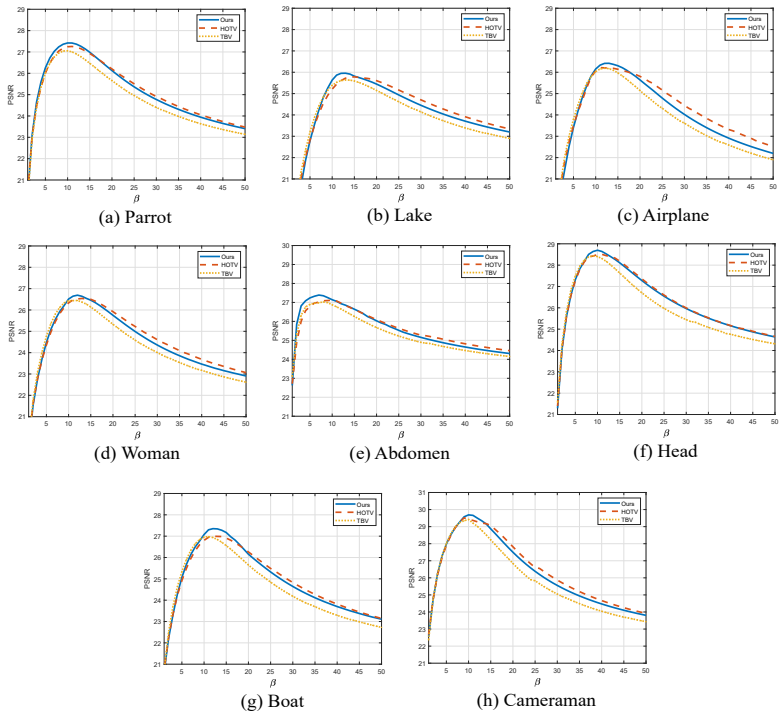

Fig. 3. Plots of the PSNR values versus the values β of the compared methods with noise level $M = 60$.

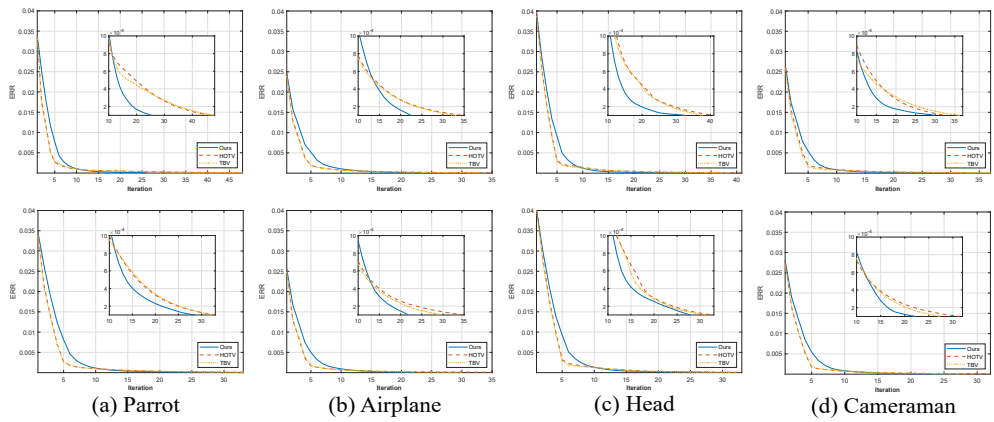

Fig. 4. Plots of the error values (ERR) versus iterations of the TV-based methods for image denoising: first row with noise level $M = 120$ and second row with noise level $M = 60$.

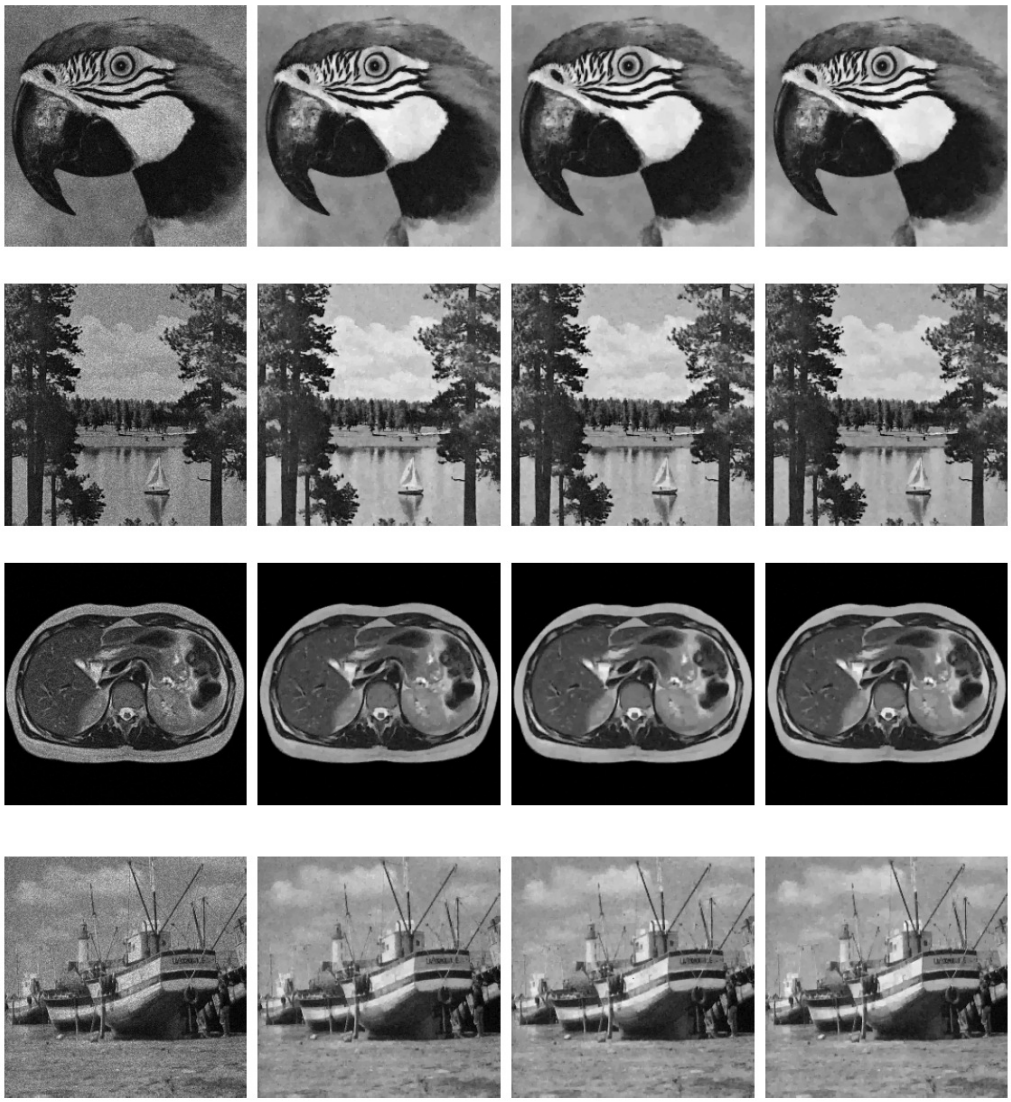

Fig. 5. Recovered images of different approaches for image denoising: a) noisy images f ($M = 120$); b) restored images by TBV approach; c) restored images by HOTV; d) restored images by our approach.

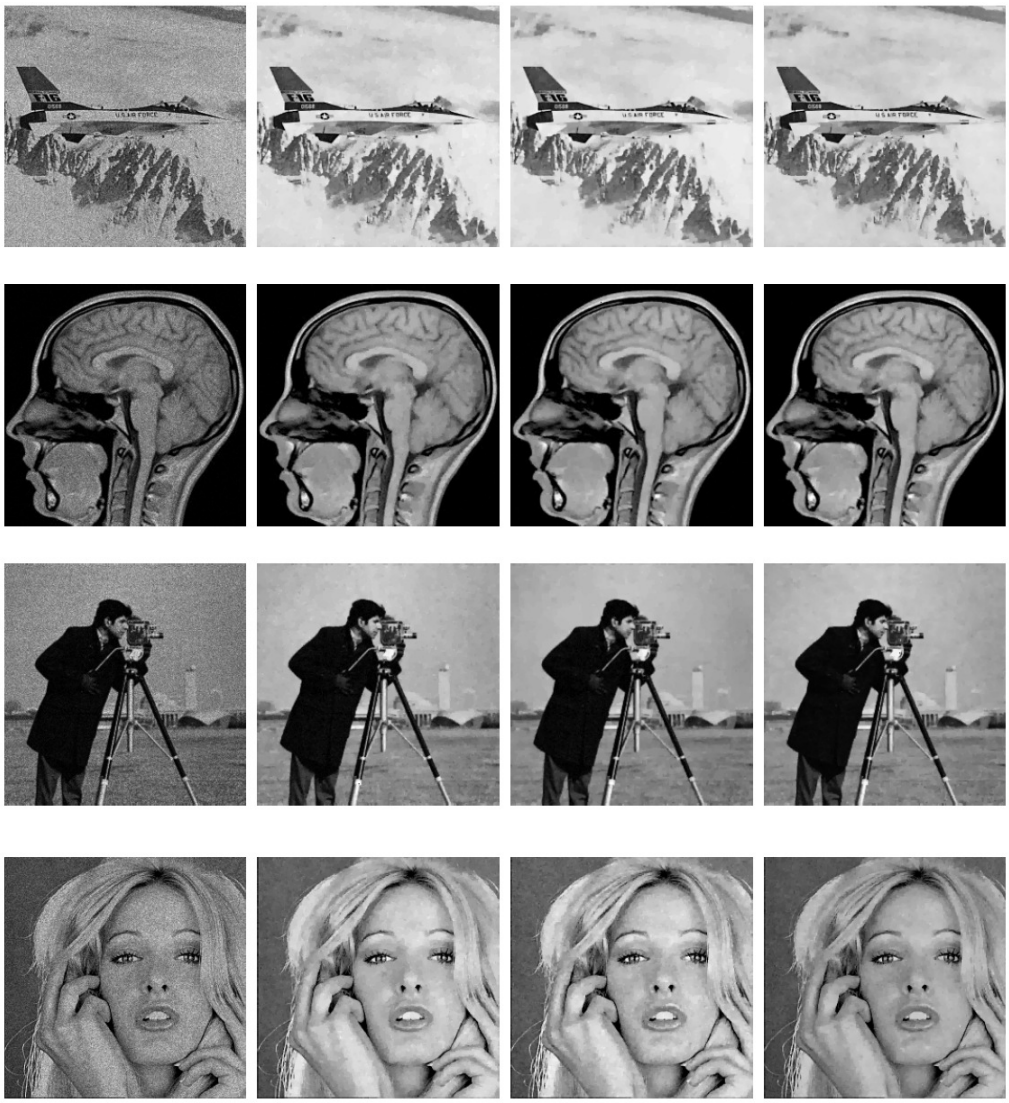

Fig. 6. Recovered images of different approaches for image denoising: a) noisy images f ($M = 120$); b) restored images by TBV approach; c) restored images by HOTV; d) restored images by our approach.

-	-	$M = 120$		$M = 60$	
Image	Method	Time (s)	N_{iter}	Time (s)	N_{iter}
Parrot	**TBV**	1.4791	48	1.0469	33
	HOTV	1.7941	47	1.3154	33
	Ours	1.1254	26	1.2431	28
Airplane	**TBV**	1.1800	34	0.9899	30
	HOTV	1.3705	35	1.3350	34
	Ours	1.0741	23	0.9027	22
Head	**TBV**	1.1991	40	1.1231	31
	HOTV	1.5484	40	1.2630	32
	Ours	1.4874	33	1.2122	28
Cameraman	**TBV**	1.1285	36	1.0097	27
	HOTV	1.3330	34	1.2837	30
	Ours	1.2604	30	1.2675	29

Tab. 2. Number of iterations and computational time of the compared methods with the optimal regularization parameter β for image denoising.

-	**PSNR**				**SSIM**			
Image	Noisy	TVB	HOTV	Ours	Noisy	BTV	HOTV	Ours
Parrot	23.8125	28.9104	28.9778	**29.1529**	0.5595	0.8635	0.8691	**0.8752**
Lake	23.7758	27.6553	27.7421	**27.9870**	0.6674	0.8580	0.8597	**0.8650**
Airplane	22.3585	28.0902	28.1409	**28.4961**	0.4879	0.8395	0.8385	**0.8469**
Woman	23.5320	28.0932	28.0101	**28.3464**	0.5661	0.7874	0.7898	**0.7917**
Abdomen	24.9110	28.2026	28.1472	**28.3992**	0.6826	0.7775	0.7833	**0.8148**
Head	25.3020	30.3857	30.4897	**30.6680**	0.6774	0.8405	0.8465	**0.8613**
Boat	23.5185	28.7211	28.6510	**28.9092**	0.5823	0.8114	0.8170	**0.8210**
Cameraman	24.1415	31.1729	31.1552	**31.5856**	0.5166	0.8749	0.8775	**0.8908**
Average	23.9190	28.9040	28.9143	**29.1931**	0.5925	0.8316	0.8352	**0.8458**

Tab. 3. PSNR values and SSIM measures for noisy images and recovered images with noise level $M = 120$.

-	**PSNR**				**SSIM**			
Image	Noisy	TVB	HOTV	Ours	Noisy	BTV	HOTV	Ours
Parrot	21.0946	27.0547	27.2575	**27.4210**	0.4446	0.8266	0.8327	**0.8394**
Lake	20.7841	25.6388	25.7850	**26.1877**	0.5748	0.8104	0.8124	**0.8140**
Airplane	19.2891	26.1889	26.2167	**26.4691**	0.3955	0.7998	0.8013	**0.8056**
Woman	20.4297	26.4447	26.5398	**26.6929**	0.4335	0.7320	0.7328	**0.7350**
Abdomen	22.6599	27.0352	27.1209	**27.3885**	0.4836	0.6271	0.6374	**0.6744**
Head	22.3923	28.4348	28.5062	**28.6983**	0.5230	0.7420	0.7518	**0.7728**
Boat	20.4660	26.9786	26.9999	**27.3516**	0.4562	0.7496	0.7567	**0.7616**
Cameraman	21.0700	29.4209	29.5184	**29.6877**	0.4083	0.8402	0.8484	**0.8622**
Average	21.0232	27.1496	27.2431	**27.4871**	0.4649	0.7660	0.7717	**0.7831**

Tab. 4. PSNR values and SSIM measures for noisy images and recovered images with noise level $M = 60$.

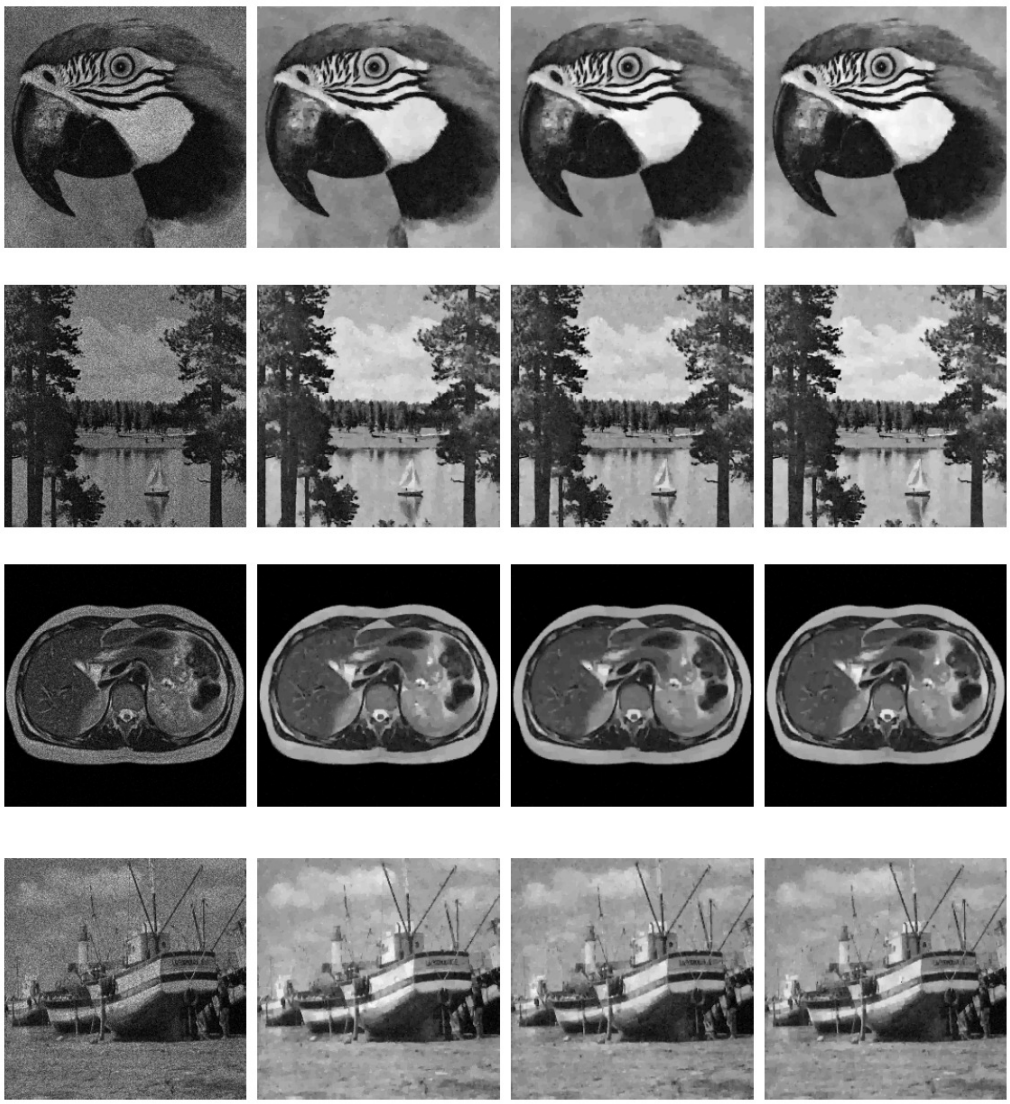

Fig. 7. Recovered images of different approaches for image denoising: a) noisy images f ($M = 60$); b) restored images by TBV approach; c) restored images by HOTV; d) restored images by our approach.

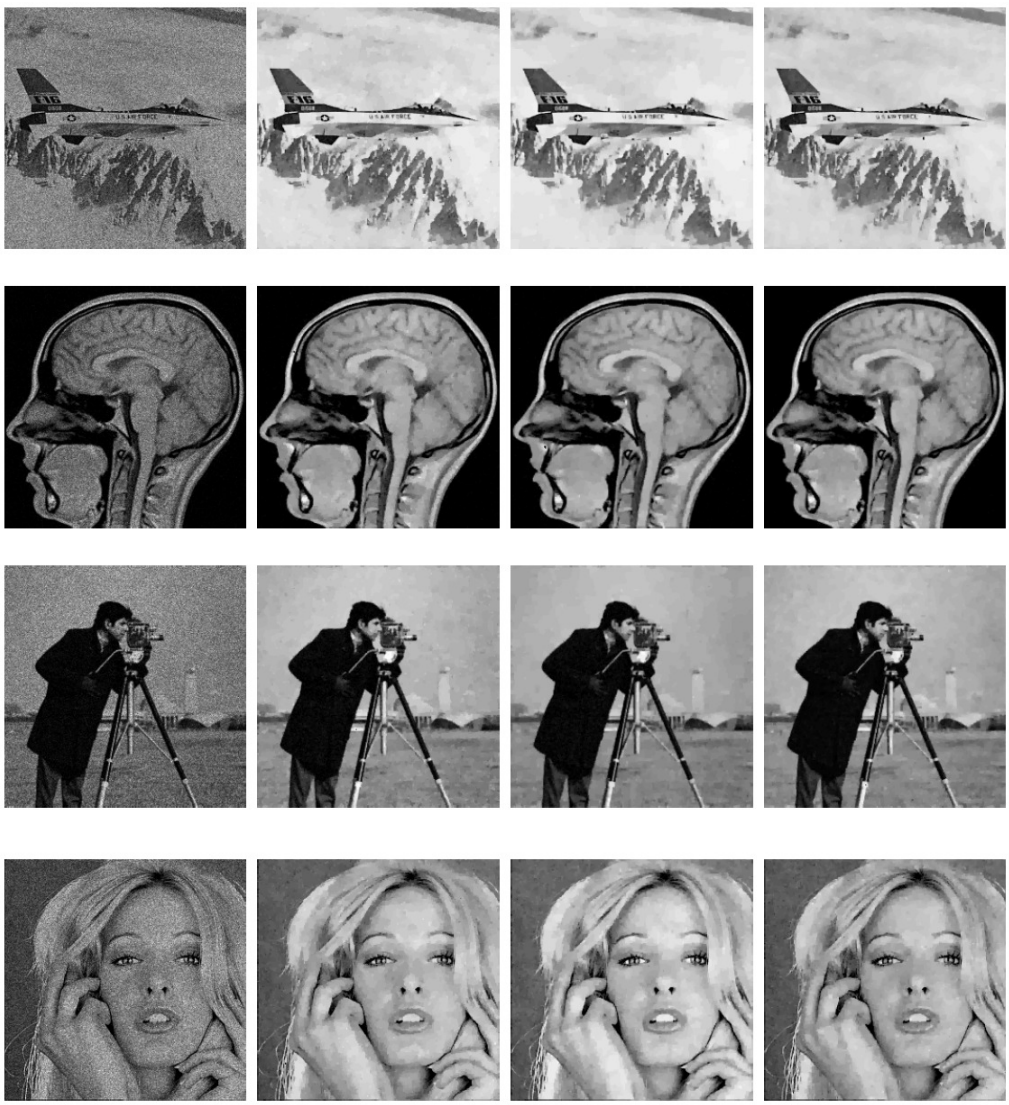

Fig. 8. Recovered images of different approaches for image denoising: a) noisy images f ($M = 60$); b) restored images by TBV approach; c) restored images by HOTV; d) restored images by our approach.

3.2. Image deblurring and denoising

In this section, we consider blurred images corrupted by Poisson noise. The blurry and noisy images are simulated as follows. The degraded images are obtained by performing the blurring operation with a window size (9×9) and standard deviation 1. After

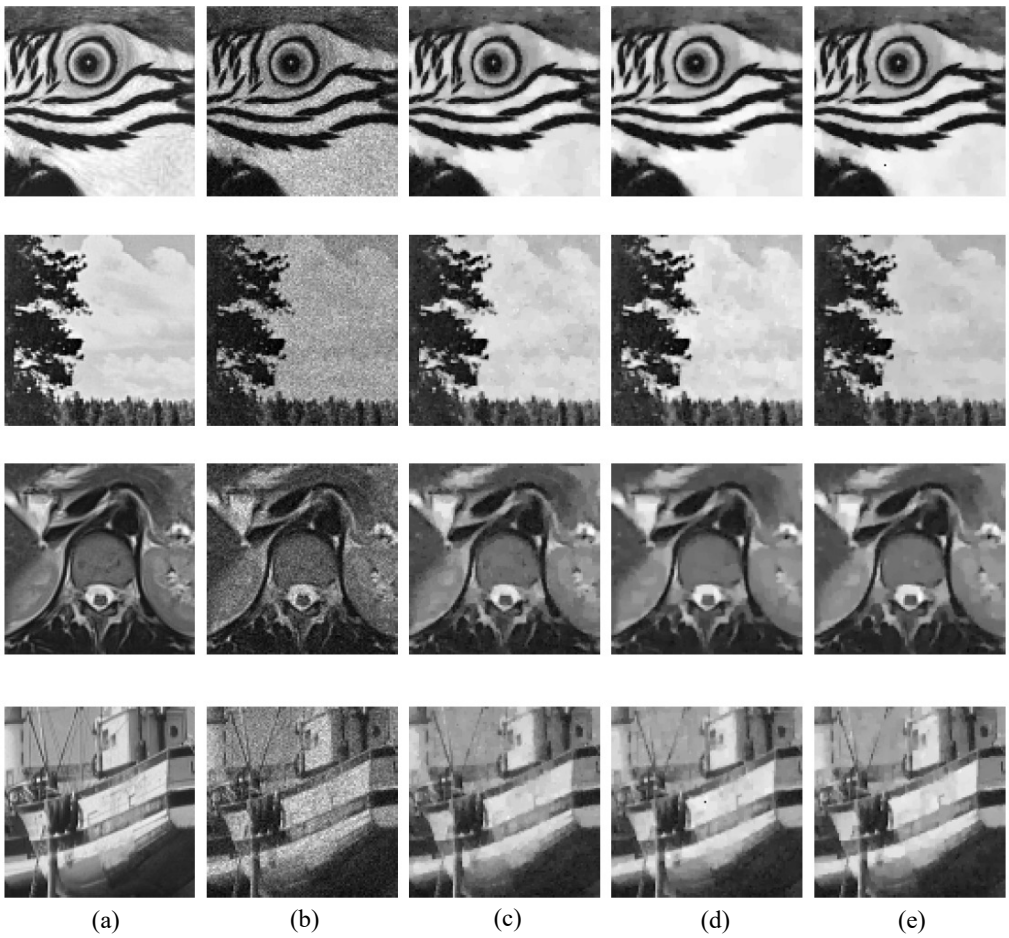

Fig. 9. The zoom-in part of the recovered image in Figure 5:
a) details of original images; b) details of noisy images f ($M = 120$);
c) details of restored images by TBV; d) details of restored images by
HOTV; e) details of restored images by our approach.

the blurring operation, we corrupt the images by adding Poisson noise with $M = 60$. Similarityly, the regularization parameter β varies from 1 to 50 by steps of 1. We plot the restored PSNR values for compared methods against different values of β (see Figure 14). The optimal values of the regularization parameters β are summarized in Table 5. In Table 6 shows the number of iterations and the computational time (in seconds) of the compared methods. In Figure 13, the evolution of ERR (18) as a function of the number of iterations for the compared methods. In Figures 15(a) and 16(a), we present the blurry and noisy images. In the others Figures 15(b) – 15(d) and 16(b) – 16(d), we show respectively the reconstructions given by the TBV, the HOTV and our model with

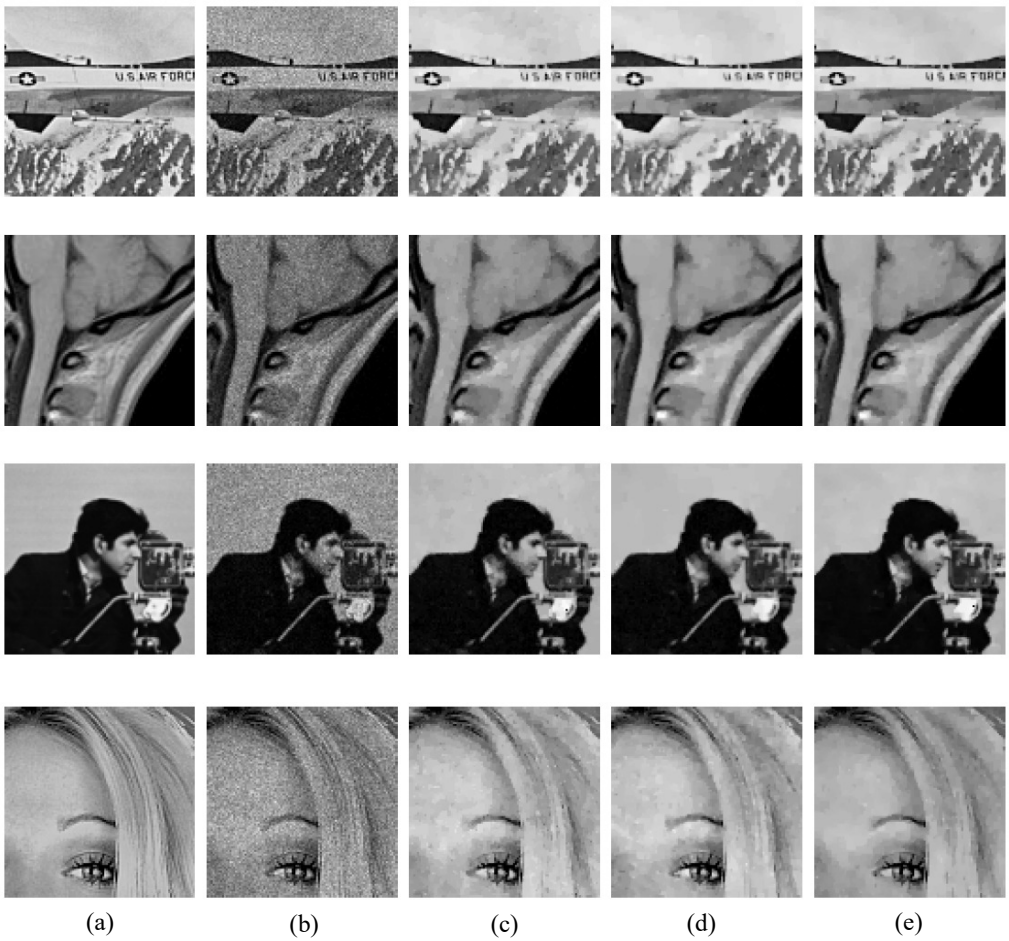

Fig. 10. The zoom-in part of the recovered image in Figure 6:
a) details of original images; b) details of noisy images f ($M = 120$);
c) details of restored images by TBV; d) details of restored images by
HOTV; e) details of restored images by our approach.

values of parameter β form Table 5, while in Figures 17 and 18 we have enlarged some details of restored images. We report the PSNR and SSIM values in Table 7.

In fact, the TBV model and the HOTV model allow good results for restoring the blurred images corrupted by Poisson noise. However, particularly, from Figures 14 – 18, we know that our proposed method has better visual quality than other methods, and from the Table 7, we know that our proposed method gets better results than other relative methods in the vast majority of cases. The numerical simulations show again that the superiority of the reconstruction quality by our proposed method for Poissonian image reconstruction.

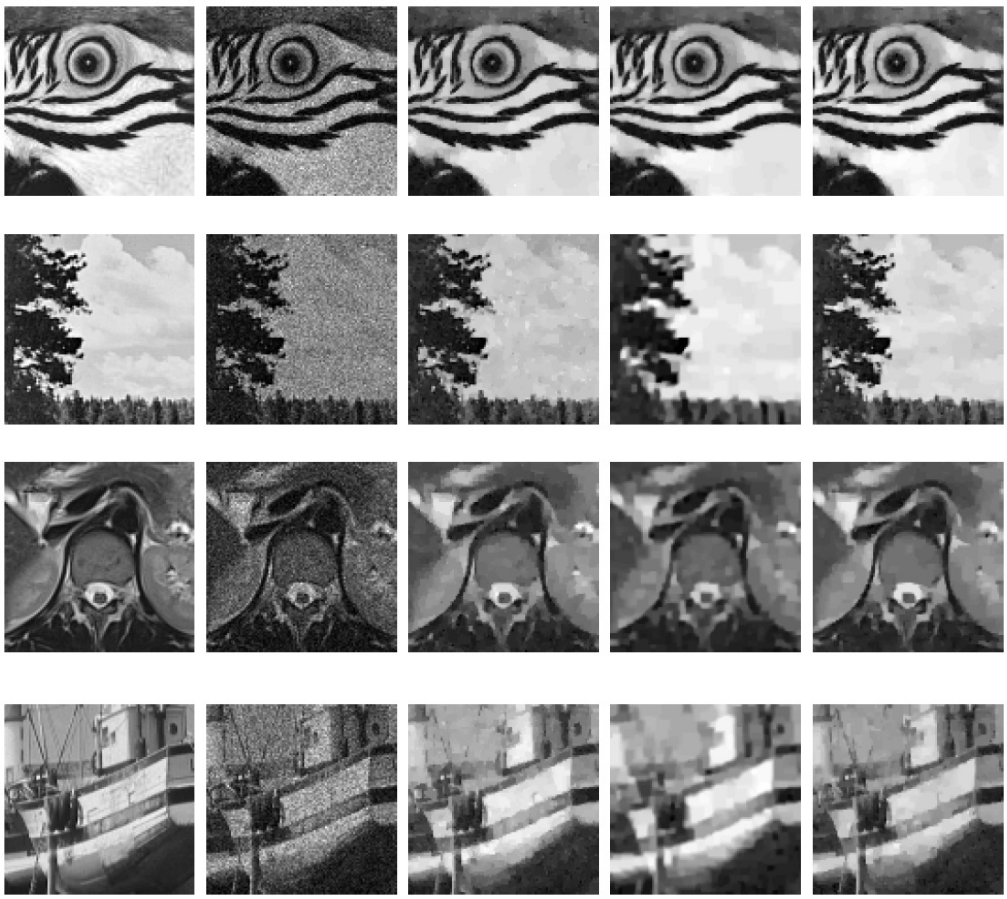

Fig. 11. The zoom-in part of the recovered image in Figure 7: a) details of original images; b) details of noisy images f ($M = 60$); c) details of restored images by TBV; d) details of restored images by HOTV; e) details of restored images by our approach.

Image	**Parrot**	**Lake**	**Airplane**	**Woman**	**Abdomen**	**Head**	**Boat**	**Cameraman**
TBV	15	23	17	1	5	8	19	16
HOTV	20	29	26	15	9	13	22	21
Ours	11	23	17	23	11	16	19	15

Tab. 5. The optimal regulization parameter β used for image deblurring and denoising.

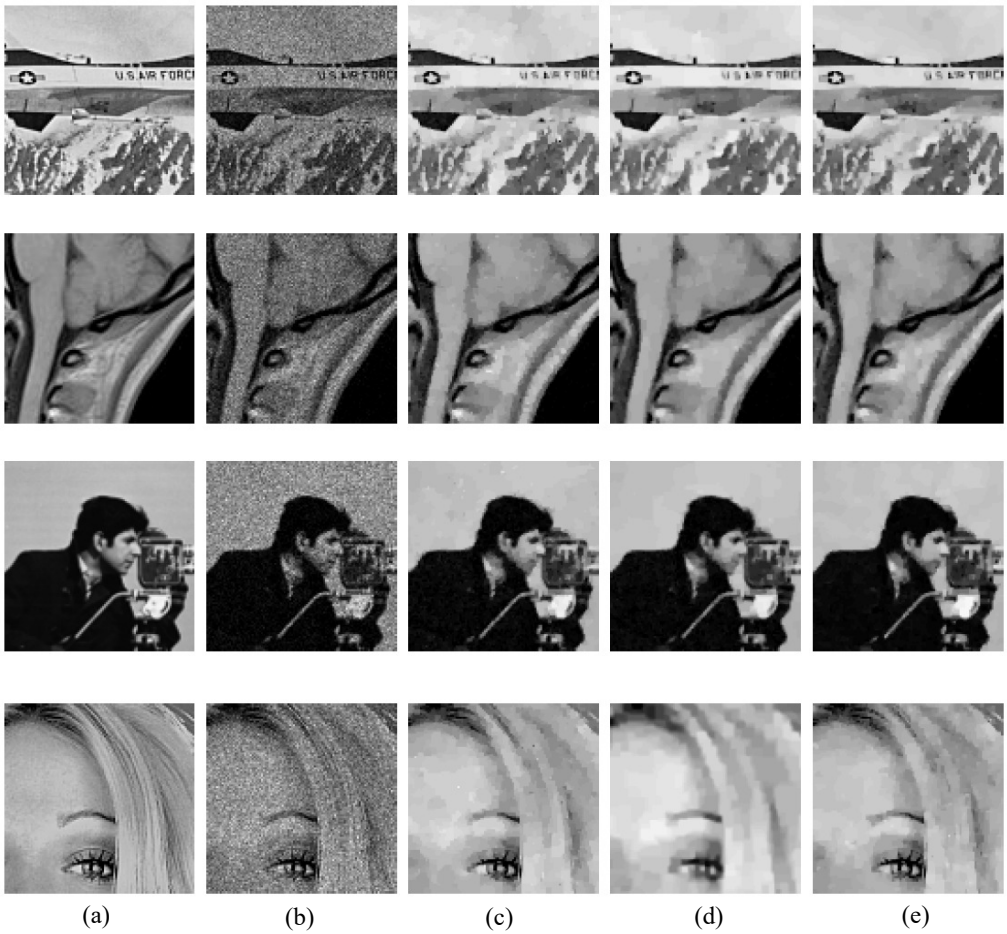

Fig. 12. The zoom-in part of the recovered image in Figure 8:
a) details of original images; b) details of noisy images f ($M = 60$);
c) details of restored images by TBV; d) details of restored images by
HOTV; e) details of restored images by our approach.

4. CONCLUSION

In this paper, we propose an adaptive variational model for deblurring and denoising of blurred images corrupted by Poisson noise. We also study the existence and the uniqueness of a solution to our proposed model. Then, applying the alternating minimization method, we solved our convex minimization problem with a convergence guarantee. The restored images show the efficiency and the capability of the proposed model, comparing to the total variation regularized based state-of-the-art techniques for deblurring and denoising of blurred images corrupted by Poisson noise.

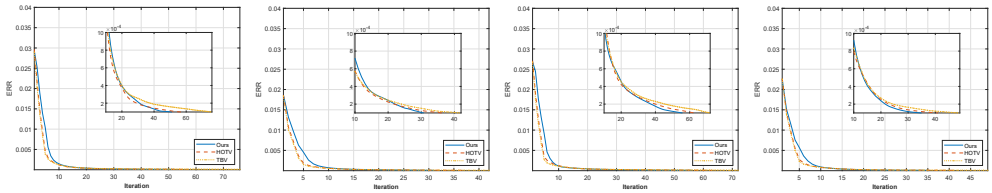

(a) Parrot (b) Airplane (c) Head (d) Cameraman

Fig. 13. Plots of the error values (ERR) versus iterations of the TV-based methods for image deblurring and denoising: the blurred images with noise level $M = 60$.

Image	Method	Time (s)	N_{iter}
Parrot	**TBV**	2.4848	79
	HOTV	2.5355	65
	Ours	2.4745	52
Airplane	**TBV**	1.5325	48
	HOTV	1.7282	44
	Ours	1.4801	32
Head	**TBV**	1.9029	61
	HOTV	2.4812	64
	Ours	1.8668	56
Cameraman	**TBV**	1.6294	52
	HOTV	1.5911	40
	Ours	1.3884	35

Tab. 6. Number of iterations and computational time of the compared methods with the optimal regularization parameter β for image deblurring and denoising.

-	**PSNR**				**SSIM**			
Image	Noisy	TVB	HOTV	Ours	Noisy	BTV	HOTV	Ours
Parrot	18.9447	21.5582	21.6389	**21.7744**	0.3692	0.7131	0.7195	**0.7265**
Lake	18.4078	21.3214	21.3762	**21.5492**	0.4097	0.6870	0.6878	**0.6929**
Airplane	16.4115	19.6087	19.4353	**20.3515**	0.2878	0.7253	0.7254	**0.7312**
Woman	14.4940	16.4635	16.0275	**16.7454**	0.2775	0.6287	0.6388	**0.6450**
Abdomen	20.1841	22.4324	22.2319	**22.6210**	0.4055	0.5712	0.5765	**0.6455**
Head	19.1146	21.7625	21.7537	**21.8819**	0.4440	0.6896	0.7057	**0.7311**
Boat	18.7125	22.5173	22.5107	**22.6898**	0.3372	0.6628	0.6735	**0.6789**
Cameraman	20.0055	26.1418	26.1915	**26.4561**	0.3497	0.8067	0.8104	**0.8173**
Average	18.2843	21.4757	21.3957	**21.7587**	0.3601	0.6856	0.6922	**0.7086**

Tab. 7. PSNR values and SSIM measures for blurred and noisy images, and recovered images with $M = 60$.

ACKNOWLEDGEMENT

The authors would like to thank Professor A. V. Kopylov, Tula State University, Tula, Russia, for his advice and comments. The authors thank the anonymous reviewers for their insightful comments and suggestions. This research is funded by Funds for Science and Technology Development of the University of Danang under project number B2019-DN02-62.

(Received February 19, 2020)

REFERENCES

[1] G. Aubert and P. Kornprobst: Mathematical Problems in Image Processing: partial differential equations and the calculus of variations. (Second edition) Applied Mathematical Science *147*, Springer–Verlag, New York 2006. DOI:

[2] J. M. Bardsley and J. Goldes: Techniques for regularization parameter and hyperparameter selection in PET and SPECT imaging. Inverse Probl. Sci. Engrg. *19* (2011), 2, 267–280. DOI:10.1080/17415977.2010.550048

[3] S. Boyd, N. Parikh, et al.: Distributed optimization and statistical learning via the alternating direction method of multipliers Found. Trends Mach. Learn. *3* (2010), 1–122.

[4] A. C. Bovik and Z. Wang: Modern Image Quality Assessment, Synthesis Lectures on Image, Video, and Multimedia Processing. Morgan and Claypool Publishers, 2006. DOI:10.2200/s00010ed1v01y200508ivm003

[5] R. H. Chan and K. Chen: Multilevel algorithm for a Poisson noise removal model with total-variation regularization. Int. J. Comput. Math. *84* (2007), 8, 1183–1198. DOI:10.1080/00207160701450390

[6] D. Q. Chen and L. Z. Cheng: Deconvolving Poissonian images by a novel hybrid variational model. J. Vis. Commun. Image R. *22* (2011), 7, 643–652. DOI:10.1016/j.jvcir.2011.07.007

[7] Y. M. Chen and T. Wunderli: Adaptive total variation for image restoration in BV space. J. Math. Anal. Appl. *272* (2002), 1, 117–137. DOI:10.1016/s0022-247x(02)00141-5

[8] F. X. Dupe, M. J. Fadili, and J L. Starck: Deconvolution of confocal microscopy images using proximal iteration and sparse representations. In: I. S. Biomed. Imaging, Paris, France (2008), pp. 736–739.

[9] I. Ekeland and R. Temam: Convex Analysis and Variational Problems. Classics in Applied Mathematics, SIAM 1999.

[10] J. Eckstein and D. P. Bertsekas: On the Douglas–Rachford splitting method and the proximal point algorithm for maximal monotone operators. Math. Programming *55* (1992), 293–318. DOI:10.1007/BF01581204

[11] I. Frosioa and N. A. Borghese: Compression and smart coding of offset and gain maps for intraoral digital x-ray sensors. Med. Phys. *36* (2009), 2, 464–479. DOI:10.1118/1.3050159

[12] C. He, C. Hu, W. Zhang, and B. Shi: A fast adaptive parameter estimation for total variation image restoration. IEEE Trans. Image Process. *23* (2014), 12, 4954–4967. DOI:10.1109/TIP.2014.2360133

[13] L. Jiang, J. Huang, X. G. Lv, and J. Liu: Restoring Poissonian images by a combined first-order and second-order variation approach. J. Math. *2013* (2013), 274573. DOI:10.1155/2013/274573

[14] L. Jiang, J. Huang, X. G. Lv, and J. Liu: Alternating direction method for the high-order total variation-based Poisson noise removal problem. Numer. Algorithms *69* (2015), 3, 495–516. DOI:10.1007/s11075-014-9908-y

[15] T. Le, R. Chartrand, and T. Asaki: A variational approach to constructing images corrupted by Poisson noise. J. Math. Imaging Vis. *27* (2007), 257–263. DOI:10.1007/s10851-007-0652-y

[16] F. Li, C. M. Shen, J. S. Fan, and C. L. Shen: Image restoration combining a total variational filter and a fourth-order filter. J. Vis. Commun. Image Res. *18* (2007), 4, 322–330. DOI:10.1016/j.jvcir.2007.04.005

[17] Q. Liu, Z. Yao, and Y. Ke: Entropy solutions for a fourth-order nonlinear degenerate problem for noise removal. Nonlinear Anal. Theor. *67* (2007), 6, 1908–1918. DOI:10.1016/j.na.2006.08.016

[18] X. Liu: Augmented Lagrangian method for total generalized variation based Poissonian image restoration. Comput. Math. Appl. *71* (2016), 8, 1694–1705. DOI:10.1016/j.camwa.2016.03.005

[19] X. Liu and L. Huang: Total bounded variation-based Poissonian images recovery by split Bregman iteration. Math. Methods Appl. Sci. *35*, (2012), 5, 520–529. DOI:10.1002/mma.1588

[20] X. Liu and L. Huang: Poissonian image reconstruction using alternating direction algorithm. J. Electronic Imaging *22* (2013), 3, 033007. DOI:10.1117/1.JEI.22.3.033007

[21] X. G. Lv, L. Jiang, and J. Liu: Deblurring Poisson noisy images by total variation with overlapping group sparsity. Appl. Math. Comput. *289* (2016), 20, 132–148. DOI:10.1016/j.amc.2016.03.029

[22] M. Ma, J. Zhang, et al.: Adaptive image restoration via a relaxed regularization of mean curvature. Math. Probl. Eng. (2020), 3416907. DOI:10.1155/2020/3416907

[23] C. A. Micchelli, L. Shen, and Y. Xu: Proximity algorithms for image models: denoising. Inverse Probl. *27* (2011), 4, 045009. DOI:10.1088/0266-5611/27/4/045009

[24] S. Osher and O. Scherzer: G–norm properties of bounded variation regularization. Commun. Math. Sci. *2* (2004), 2, 237–254. DOI:10.4310/cms.2004.v2.n2.a6

[25] A. Padcharoen, P. Kumama, and J. Martinez-Moreno: Augmented Lagrangian method for TV-$l1$-$l2$ based colour image restoration. J. Comput. Appl. Math.*354* (2019), 507–519. DOI:10.1016/j.cam.2018.09.053

[26] C. T. Pham and A. Kopylov: Multi-quadratic dynamic programming procedure of edge-preserving denoising for medical images. Int. Arch. Photogramm. Remote Sens. Spatial Inf. Sci. *XL-5/W6* (2015), 101–106. DOI:10.5194/isprsarchives-XL-5-W6-101-2015

[27] C. T. Pham, G. Gamard, A. Kopylov, and T. T. T. Tran: An algorithm for image restoration with mixed noise using total variation regularization. Turk. J. Elec. Eng. Comp. Sci. *26* (2018), 2832–2846. DOI:10.3906/elk-1803-100

[28] C. T. Pham and A. V. Kopylov: Tree-serial parametric dynamic programming with flexible prior model for image denoising. Comput. Opt. *42* (2018), 838–845. DOI:10.1002/gepi.22154

[29] C. T. Pham, T. T. T. Tran, et. al.: An adaptive algorithm for restoring image corrupted by mixed noise. Cybern. Phys. *8* (2019), 73–82. DOI:10.35470/2226-4116-2019-8-2-73-82

[30] C. T. Pham, T. T. T. Tran, and G. Gamard: An efficient total variation minimization method for image restoration. Informatica *31* (2020), 539–560. DOI:10.15388/20-infor407

[31] P. Sarder and A. Nehorai: Deconvolution method for 3D fluorescence microscopy images. IEEE Signal Process. Magazine *23* (2006), 3, 32–45. DOI:10.1109/MSP.2006.1628876

[32] A. Sawatzky, C. Brune, T. Kasters, F. Wabbeling, and M. Burger: EM-TV methods for inverse problems with Poisson noise. Lect. Notes Math. Springer *2090* (2013), 71–142. DOI:10.1007/978-3-319-01712-9_2

[33] S. Setzer, G. Steidl, T. Teuber: Deblurring Poissonian images by split Bregman techniques. J. Vis. Commun. Image R. *21* (2010), 3, 193-199. DOI:10.1016/j.jvcir.2009.10.006

[34] M. Yan: EM-type algorithms for image reconstruction with background emission and Poisson noise. Lect. Notes Comput. Sci. Springer Berlin Heidelberg *6938* (2011), 33–42. DOI:10.1007/978-3-642-24028-7_4

[35] J. Zhang, M. Ma, Z. Wu, and C. Deng: High-order total bounded variation model and its fast algorithm for poissonian image restoration. Math. Probl. Engrg. (2019), 2502731. DOI:10.1155/2019/2502731

[36] Y. Wang, J. Yang, W. Yin, Y. Zhang: A new alternating minimization algorithm for total variation image reconstruction. SIAM J. Imaging Sci. *1* (2008), 3, 248-272. DOI:10.1137/080724265

[37] Y. Wen, R. H. Chan, and T. Zeng: Primal-dual algorithms for total variation based image restoration under Poisson noise. Sci. China Math. *59* (2016), 141–160. DOI:10.1007/s11425-015-5079-0

[38] H. Woo and S. Yun: Alternating minimization algorithm for speckle reduction with a shifting technique. IEEE T. Image Process. *21* (2012), 1701–1714. DOI:10.1109/TIP.2011.2176345

Cong Thang Pham, Corresponding author. The University of Danang - University of Science and Technology, 54 Nguyen Luong Bang Street, Danang City. Vietnam.
e-mail: pcthang@dut.udn.vn

Thi Thu Thao Tran, The University of Danang – University of Economics, 71 Ngu Hanh Son Street, Danang City. Vietnam.
e-mail: thaotran@due.udn.vn

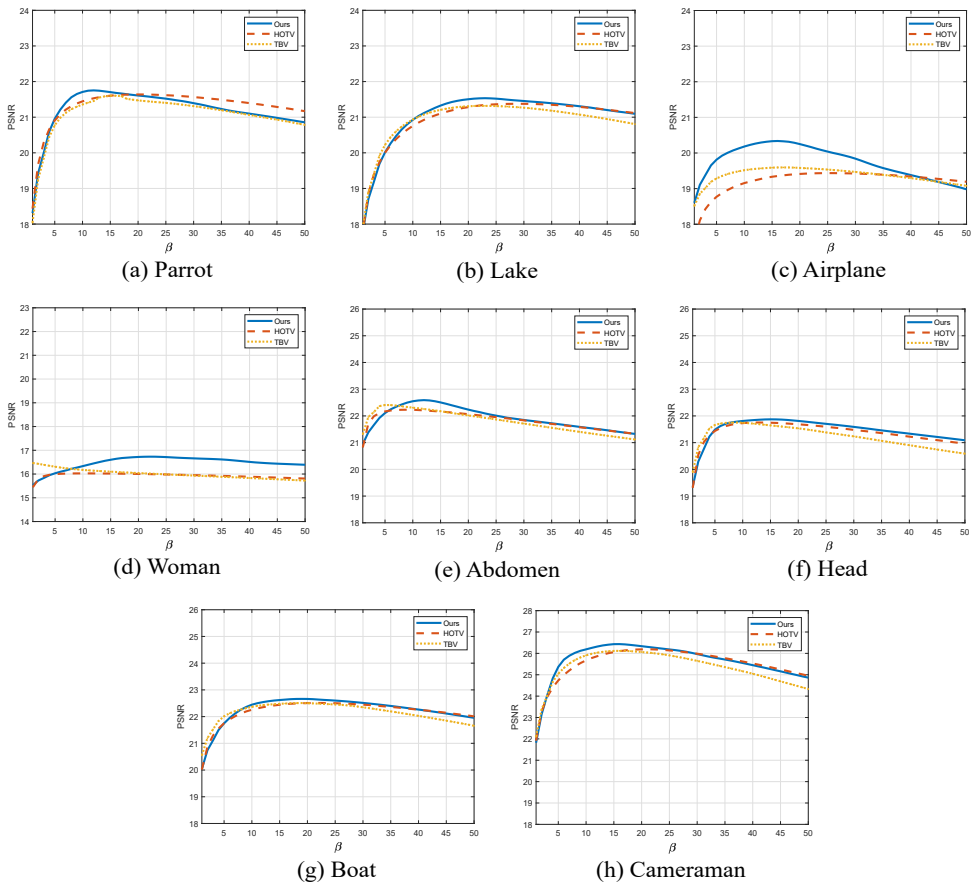

Fig. 14. Plots of the PSNR values versus the values β of the compared methods for image deblurring and denoising: the blurred images with noise level $M = 60$.

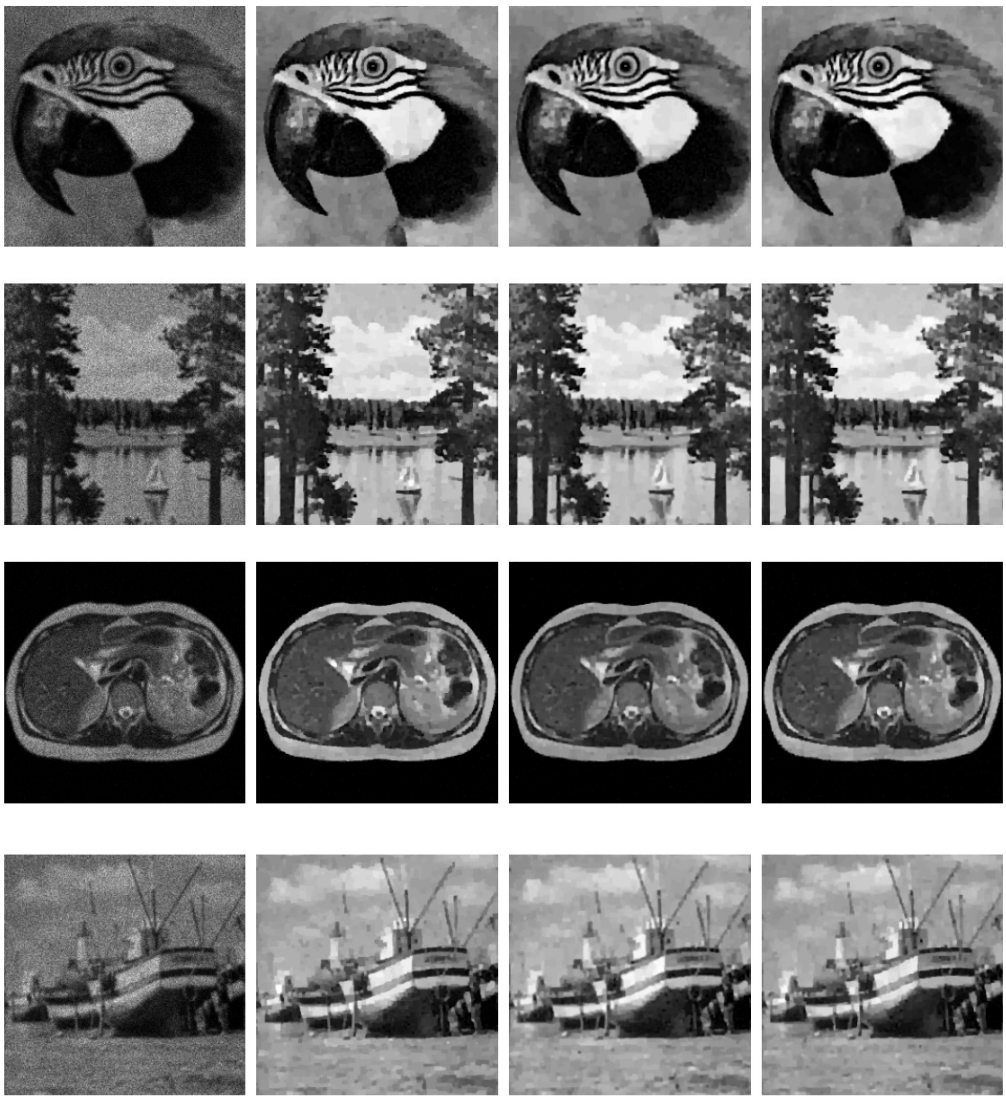

(a) (b) (c) (d)

Fig. 15. Recovered images of different approaches for deblurring and denoising:
a) blurred and noisy images with $M = 60$; b) restored images by TBV approach;
c) restored images by HOTV; d) restored images by our approach.

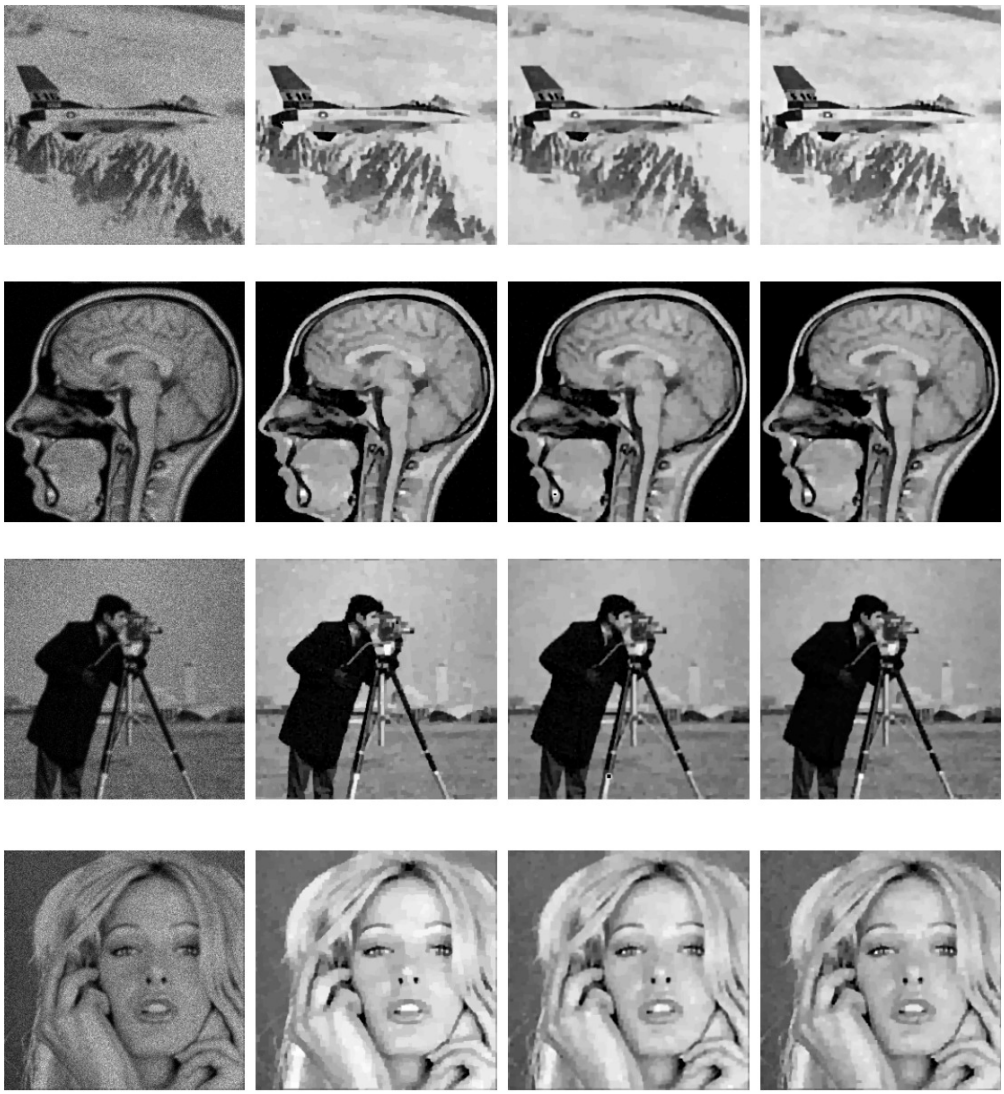

Fig. 16. Recovered images of different approaches for deblurring and denoising:
a) blurred and noisy images with $M = 60$; b) restored images by TBV approach;
c) restored images by HOTV; d) restored images by our approach.

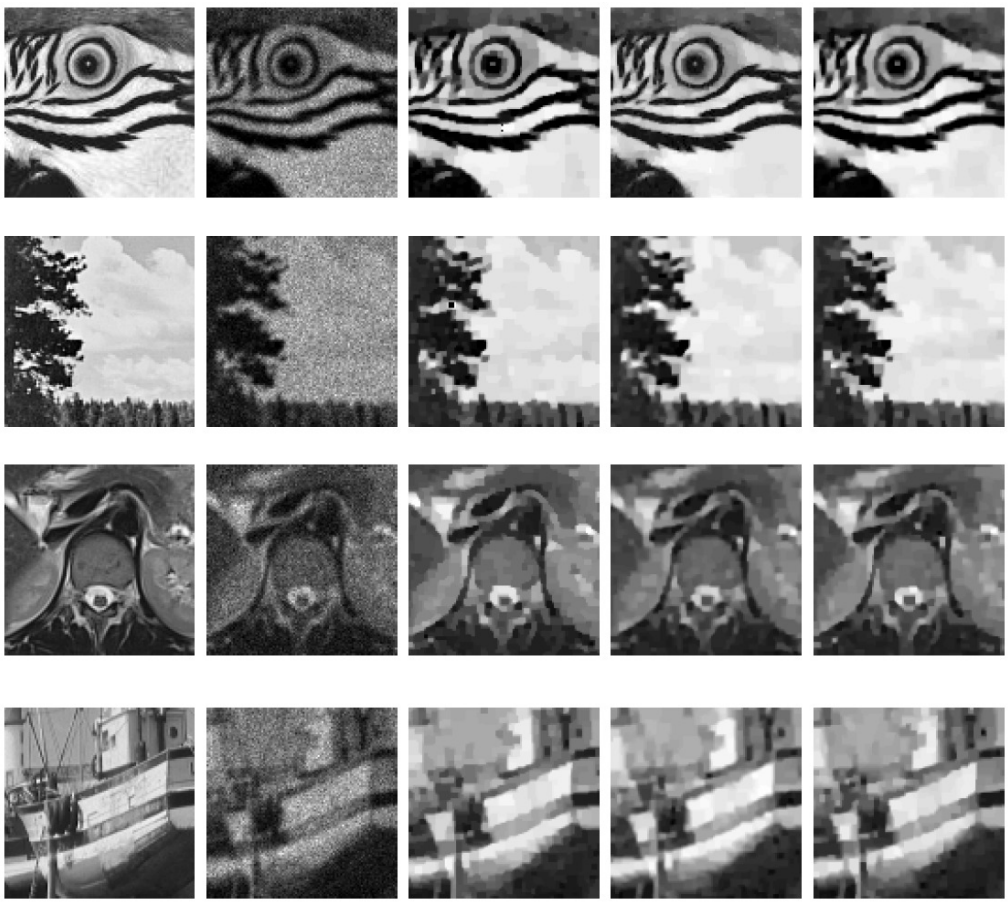

Fig. 17. The zoom-in part of the recovered image in Figure 15:
a) details of original images; b) details of noisy images f ($M = 60$);
c) details of restored images by TBV; d) details of restored images by
HOTV; e) details of restored images by our approach.

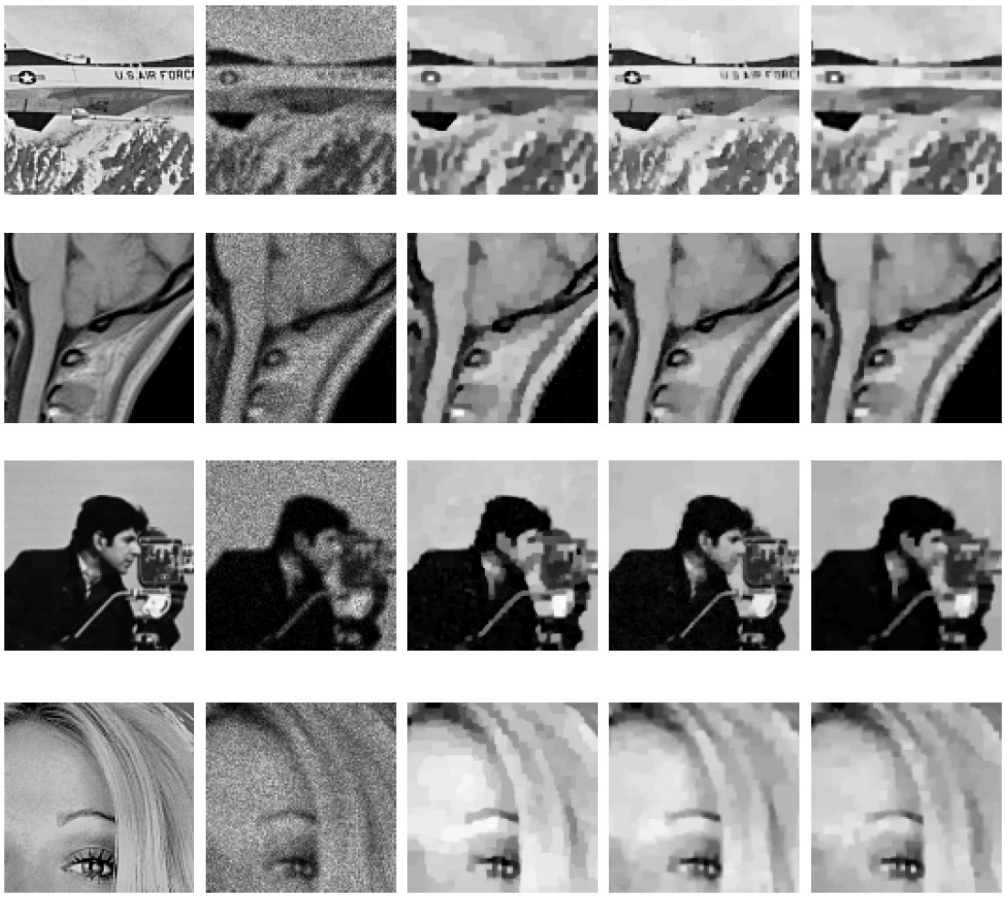

Fig. 18. The zoom-in part of the recovered image in Figure 16:
a) details of original images; b) details of noisy images f ($M = 60$);
c) details of restored images by TBV; d) details of restored images by
HOTV; e) details of restored images by our approach.